PHYSICAL REVIEW E **93**, 041102(R) (2016)

Suppression mechanism of Kelvin-Helmholtz instability in compressible fluid flows

Mona Karimi[1,2,*] and Sharath S. Girimaji[2]

[1]*Department of Mathematics, Texas A&M University, College Station, Texas 77843, USA*

[2]*Aerospace Engineering Department, Texas A&M University, College Station, Texas 77843, USA*

(Received 12 July 2015; revised manuscript received 24 March 2016; published 18 April 2016)

The transformative influence of compressibility on the Kelvin-Helmholtz instability (KHI) at the interface between two fluid streams of different velocities is explicated. When the velocity difference is small (subsonic), shear effects dominate the interface flow dynamics causing monotonic roll-up of vorticity and mixing between the two streams leading to the KHI. We find that at supersonic speed differentials, compressibility forces the dominance of dilatational (acoustic) rather than shear dynamics at the interface. Within this dilatational interface layer, traveling pressure waves cause the velocity perturbations to become oscillatory. We demonstrate that the oscillatory fluid motion reverses vortex roll-up and segregates the two streams leading to KHI suppression. Analysis and illustrations of the compressibility-induced suppression mechanism are presented.

DOI: 10.1103/PhysRevE.93.041102

Kelvin-Helmholtz instability (KHI) [1,2] occurs at the interface of any two fluid streams in a state of relative motion or stratification [3]. The flow dynamics underlying the three-stage development of KHI in low-speed shear layers—highlighted by vortex roll-up and intense mixing between two streams—is well established in literature [4]. The KHI in compressible flows is of much importance in astrophysical jets [5–7], protoplanetary disks [8], other natural flows [9–13], and engineering applications [14,15]. It has long been known that KHI is suppressed in compressible flows [16–21]. Yet, identifying the fundamental physical mechanism responsible for vortex roll-up disruption and mixing inhibition remains an unsolved problem. It is evident that the suppression must be due to the transformation in character of pressure from an incompressibility preserving Lagrange multiplier at low speeds to a *bona fide* thermodynamic state variable at high speeds. Eigenmode analyses [19,22–26] that clearly indicate asymptotic KHI inhibition are inherently unsuited for explaining the transient suppressing action of pressure. A clear understanding of the transient pressure effects culminating in KHI suppression is critical for predicting transition and turbulence in high-speed shear flows.

In this work, we explain the transient suppression mechanism employing (linear) initial value analysis and numerical simulations. We examine the interplay between pressure, velocity, and vorticity fields at different speed regimes. The focus is on the wave character of pressure at high speeds and the consequent effect on vortex dynamics. We will demonstrate that the compressible pressure-vorticity dynamics undergoes a drastic change resulting in inhibition of mixing across the interface and suppression of instability.

Three-dimensional inviscid compressible Navier-Stokes equations form the basis of this analysis [17,27–29]. The flow and thermodynamic variables (velocity field, $\mathbf{u}$; pressure, p; density, ρ; and temperature, T) are decomposed into base and perturbation fields: $q(\rho,u_i,p)=\bar{q}+q'$. The base or background velocity is described by a steady, planar, parallel free-shear layer $\bar{\mathbf{u}}=(U_1(x_2),0,0)$. Here, x_1, x_2, and x_3 are taken to be the streamwise, normal and spanwise directions.

For a planar shear layer, $\partial\bar{p}/\partial x_i=0$ and $\partial\bar{u}_i/\partial x_i=0$ [29]. The evolution of the perturbation field is most rigorously examined in a reference frame advecting with the unperturbed flow [30]: $X_1=x_1-\int_0^t U_1 d\xi$, $X_2=x_2$, and $X_3=x_3$. The linearized equations of the perturbation evolution described in the new coordinate frame are

$$\frac{\partial u_1'}{\partial t}=-\frac{\partial(p'/\bar{\rho})}{\partial X_1}-u_2'S, \tag{1}$$

$$\frac{\partial u_2'}{\partial t}=-\frac{\partial(p'/\bar{\rho})}{\partial X_2}-\frac{\partial(p'/\bar{\rho})}{\partial X_1}S^*, \tag{2}$$

$$\frac{\partial u_3'}{\partial t}=-\frac{\partial(p'/\bar{\rho})}{\partial X_3}, \tag{3}$$

$$\frac{\partial p'}{\partial t}=-\gamma\bar{p}\left[\frac{\partial u_1'}{\partial X_1}-\frac{\partial u_2'}{\partial X_1}S^*+\frac{\partial u_2'}{\partial X_2}+\frac{\partial u_3'}{\partial X_3}\right], \tag{4}$$

$$\frac{\partial\omega_3'}{\partial t}\approx -u_2'\frac{\partial S}{\partial X_2}+\left[\frac{\partial u_1'}{\partial X_1}+(1-S^*)\frac{\partial u_2'}{\partial X_2}\right]S, \tag{5}$$

where $S=\partial_{X_2}U_1$ is the background shear rate and $S^*=\int_0^t S(X_2)d\xi$. The specific heat ratio is γ, and p is given by the ideal gas law, $p=\rho RT$. Inspection of the linearized equations shows that (i) the growth of perturbation kinetic energy and spanwise vorticity (ω_3') depends principally on u_2'; and (ii) the effect of change in the character of p' on u_2' holds the key to understanding the compressibility suppression mechanism.

To extract the nonmodal stabilization mechanism [31], we perform an *initial value analysis*. Hence, we examine the temporal evolution of the two-dimensional perturbation mode of the type $q=\hat{q}(X_2,t)e^{i\kappa_1 X_1}$, where $\hat{(\cdot)}$ is the Fourier amplitude, κ_1 is the streamwise wave number, and $\hat{q}(X_2,0)$ satisfies the free-stream boundary conditions. To examine the compressibility effect manifesting *via* the p'-u_2' interaction, (2)–(4) is rearranged in the form of wave (hyperbolic) equations with source terms [32]:

$$M_g^2\frac{\partial^2\hat{p}^*}{\partial t^{*2}}=\frac{\partial^2\hat{p}^*}{\partial x_2^{*2}}-\hat{p}^*+2i\frac{u_0\bar{\rho}}{\kappa\bar{p}}\hat{u}_2^*S, \tag{6}$$

$$M_g^2\frac{\partial^2\hat{u}_2^*}{\partial t^{*2}}=\frac{\partial^2\hat{u}_2^*}{\partial x_2^{*2}}+(\hat{u}_2^*S^*-\hat{u}_1^*)S^*+\frac{i}{\kappa}\frac{\hat{p}^*}{\gamma u_0}S, \tag{7}$$

*mona.karimi@tamu.edu

where $M_g = S/\bar{a}_0\kappa$ is the *gradient Mach number* [33] and $\bar{a}_0 = \sqrt{\gamma\bar{p}/\bar{\rho}}$ is the speed of sound. The independent variables are normalized as follows: $t^* = St$ and $x_2^* = \kappa X_2$, where κ is the magnitude of the perturbation wave number. The normalized pressure and velocity amplitudes are $\hat{p}^* = \hat{p}/\bar{p}$ and $\hat{u}_i^* = \hat{u}_i/u_0$, respectively, where u_0 is the root mean square of the initial perturbation velocity. From the dimensionless form of (6) and (7), it is evident that M_g is the relevant Mach number to characterize compressibility effects on the perturbation field.

The time scale of pressure constitutes the biggest difference between incompressible and compressible flows. A reasonable analytical estimate of the pressure time scale can be obtained by invoking WKB-like approximation [34] into Eqs. (6) and (7), which suppresses spatial variations in shear. Now Eqs. (6) and (7) reduce to a third-order ordinary differential equation for pressure:

$$\frac{d^3\hat{p}^*}{dt^{*3}} = -\frac{1}{M_g^2}\left(\frac{d\hat{p}^*}{dt^*} + \frac{2\kappa_2}{\kappa}\hat{p}^*\right). \tag{8}$$

The solution of Eq. (8) for the case of the compressible homogeneous shear flows can be obtained by using generalized hypergeometric functions, such as Bessel functions [35]. Ultimately, the asymptotic expansion of solution indicates that the pressure amplitude oscillates in time.

However, for the early and intermediate times of the perturbation evolution of the pressure amplitude, Eq. (8) permits a solution of the type [36]

$$\hat{p}^* \approx \hat{p}_0^* e^{[\sigma(t)/S]t^*};$$
$$\frac{\sigma(t)}{S} \sim \begin{cases} \frac{1}{M_g^{2/3}}t^{*1/3}, & \text{early time} \\ \frac{1}{M_g}t^*, & \text{intermediate time,} \end{cases} \tag{9}$$

where σ is the frequency of pressure-amplitude variation. At low Mach numbers ($M_g \to 0$) σ is very large at all times (9) and the time scale of pressure evolution is very small leading to the well-known Poisson equation for pressure. It can then be shown that the behavior u_2' is monotonic resulting in the sustained growth of perturbation vorticity and kinetic energy (4) resulting in familiar KHI behavior. At high speeds ($M_g > 1$), p' evolution is described by the nonhomogeneous wave equation and pressure propagates through the flow field at a wave speed proportional to $1/M_g$. It is immediately evident that u_2' which is coupled as a harmonic oscillator also attains the wavelike character in compressible flows. The changing sign of u_2' in a compressible shear layer has a profound effect on perturbation kinetic energy and spanwise vorticity. At any given location, the production of both these flow features will alternate in sign as S and $\partial_{X_2}S$ in the vorticity equation (4) are nearly constant. Thus, we can conclude from the analysis of the reduced mathematical equations that spanwise vortex structures roll and unroll repeatedly. Furthermore, perturbation energy production is alternately positive and negative. Such behavior will necessarily result in stabilization of the flow.

To explore the stabilizing interplay between pressure, velocity, and ultimately vorticity more precisely, we perform direct numerical simulations of perturbation evolution in a temporally evolving mixing layer. Nonlinear and viscous effects omitted in the simplified analysis are now included,

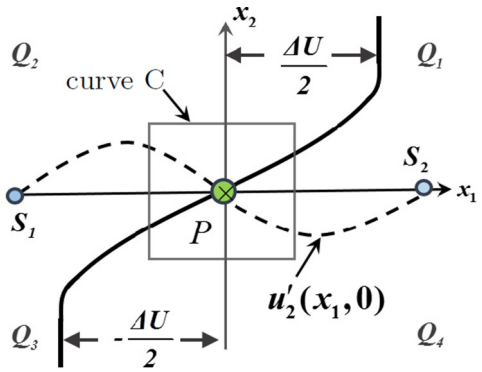

FIG. 1. A schematic of a mixing layer with the initial perturbation of $u_2'(x_1, t = 0)$; pivot point P; stagnation points S_1, S_2; and quadrants marked by Q_1–Q_4.

resulting in a more comprehensive investigation. The goals are to (i) examine KHI in compressible flows and (ii) contrast the KH dynamics at low and high Mach numbers. The numerical scheme has been thoroughly validated [32,36–38]. The base velocity field features the requisite inflection point: $\bar{u}_i = (\Delta U/2\tanh(0.5x_2/\delta_m^0),0,0)$, where δ_m^0 is the initial momentum thickness of the mixing layer. Even at very high speeds, it is evident from (6) and (7) that high wave-number perturbations ($\kappa > S/\bar{a}_0$) experience subsonic M_g. Therefore, a low-wave-number or large-wavelength initial velocity perturbation field is chosen: $u_i' = (0,\hat{u}_2^0\sin(\kappa_1 x_1),0)$; $\kappa_1 = 2\pi/L = 1$ and 2, where L is the domain length and the initial perturbation amplitude, $\hat{u}_2^0 = 0.05\Delta U$. The thermodynamic fields are initially taken to be uniform. The simulations are carried out for the air ($\gamma = 1.4$), with the initial values of Prandtl and Reynolds numbers: $\mathrm{Pr} = 0.7$ and $\mathrm{Re}_{\delta_m^0} = 400$. Mixing layers of different convective Mach number are computed: $M_c = \Delta U/2\bar{a} = 0.3$, 0.6, 0.8, 1.0, 1.1, and 1.2. It must be noted that the convective Mach number M_c is a global measure of the mixing layer speed, while M_g is a local measure of the effect of compressibility on the perturbation of wave number κ.

A thorough numerical convergence study confirms that a cubic domain of side $L = 2\pi$ with $256 \times 512 \times 128$ grid points provides results of requisite accuracy [32]. Various features of the computational geometry and flow conditions are exhibited in Fig. 1. The extent of KHI can be characterized in terms of the following mixing metrics: (i) momentum thickness $\delta_m = (1/\bar{\rho}_0)\int_{-\infty}^{\infty}\bar{\rho}(1/4 - u_1^2/\Delta U^2)dx_2$, (ii) perturbation turbulent kinetic energy, and (iii) circulation: $\Gamma = \oint_C \vec{u}' \cdot d\vec{l}$ where $d\vec{l}$ is a directed line segment and C is a square of side $\pi/2$ centered at the inflection point of the mean velocity profile, shown in Fig. 1. The evolution of these metrics obtained from the simulations are presented for different Mach numbers in Fig. 2.

Consistent with the findings in literature [20,39–44], we find that all mixing characteristics monotonically diminish with the Mach number indicating a gradual suppression of KHI with increasing M_c (Fig. 2). To highlight the difference between high and low Mach number effects, we examine p'-u_2'-ω_3' interactions at the two extreme Mach number cases. We begin with a brief description of the incompressible instability mechanism and contrast it against the compressible-case behavior.

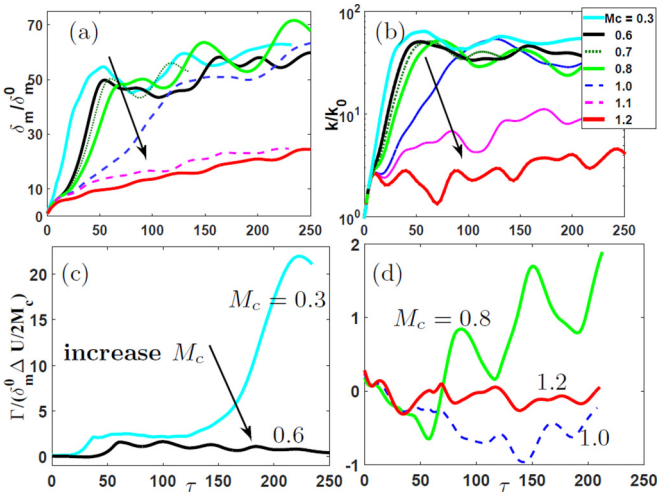

FIG. 2. The temporal evolution of the mixing metrics: momentum thickness (a), turbulent kinetic energy (b), and circulation around the inflection point of the base velocity at low and high M_c, (c) and (d), respectively. Horizontal axis is the normalized time: $\tau = t\Delta U/\delta_m^0$.

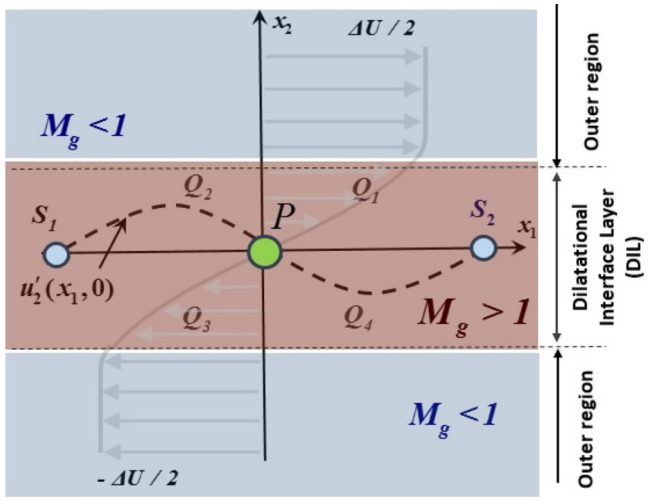

FIG. 4. Schematic of a compressible mixing layer. The initial perturbation profile—$u_2'(x_1,0)$—and the DIL are shown. Stagnation points (P, S_1, and S_2) and quadrants (Q_1–Q_4) are also identified.

Development of KHI in the incompressible flows. For this case, $M_g \ll 1$ nearly everywhere in the mixing layer. It can be shown that perturbation fields evolve monotonically leading to the formation of the classical KHI which abides by the Rayleigh inflection point criterion [28]. The three stages of instability development [45,46] can be identified referring to Fig. 3 which shows the p' and ω_3' contours at various times. The dynamics in the four quadrants (Q_1–Q_4) around the stagnation point P and the neighborhood of points S_1 and S_2, schematically shown in Fig. 4, are central to this description.

Stage 1. In the *initial development* stage, a low-pressure region forms around P and high-pressure regions form around S_1 and S_2 due to initial conditions. In the neighborhood of the pivot point P, negative (clockwise) vortices are initiated in quadrants Q_2 and Q_4, and positive (counterclockwise) vortices in Q_1 and Q_3. These features are captured in Figs. 3(a) and 3(b).

Stage 2. In the region around P, the Poisson character of pressure leads to a positive-feedback interaction between

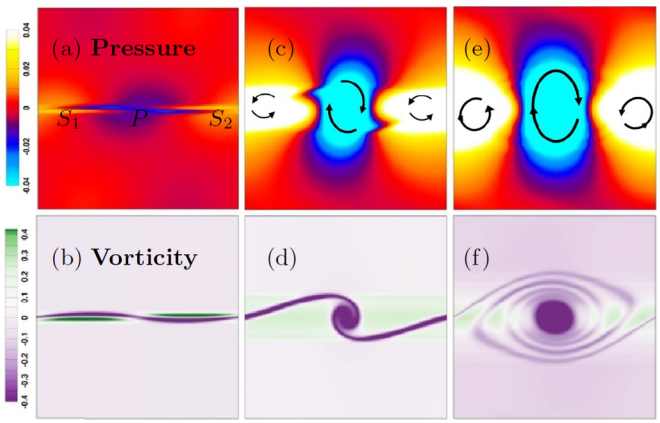

FIG. 3. KHI development in the incompressible ($M_c = 0.3$) case: *Stage 1*—initial development [(a), (b)]; *Stage 2*—merger and roll-up [(c) and (d)]; and *Stage 3*—asymptotic [(e)–(f)].

clockwise vorticity and decreasing pressure. Low pressure and clockwise vorticity mutually intensify each other in Q_2 amd Q_4. On the contrary, pressure weakens counterclockwise vortices in Q_1 and Q_3. As a result, the two negative vortices grow and merge in the vicinity of P. The merged clockwise vortex begins to roll-up rapidly constituting the central mechanism of KHI evolution known as the *merger and roll-up* stage. The rolling vortex begins to entrain fluid from both free streams [Figs. 3(c) and 3(d)]. At S_1 and S_2, high pressure leads to suppression of the clockwise vortex and mild enhancement of the counterclockwise vortex. Thus, the pressure and vorticity fields grow slowly at these points.

Stage 3. The *nonlinear asymptotic* KHI stage is marked by consolidation and rapid inward spiral rotation of the low-pressure vortex around the pivot point P. Entrainment intensifies leading to the onset of instability as can be seen from Figs. 3(e) and 3(f).

Development KHI in the compressible flows. At high M_c, there exists a region around the interface within which $M_g(x_2)$ exceeds unity—which we call *dilatational interface layer* (DIL).

Within the DIL, p' and u_2' exhibit strong wavelike character (6) and (7). In the outer regions, where $M_g(x_2) < 1$, the wave character of p' and u_2' is much weaker. A schematic of a typical compressible mixing layer is shown in Fig. 4.

To understand the wave character of the DIL upon KHI, contours of pressure and vorticity perturbations for the $M_c = 1.2$ case are presented in Fig. 5. The DIL can be identified as the narrow region in the middle, in Figs. 5(c)–5(e). The different stages of perturbation evolution at high M_c are as follows.

Stage 1. The *initial development* stage of the compressible mixing layer is similar to that of the incompressible case as the initial conditions are identical: low pressure forms around P and high pressure around S_1 and S_2. The similarities of this stage at different Mach numbers can be seen from Figs. 3(a) and 3(b) and Figs. 5(a) and 5(b).

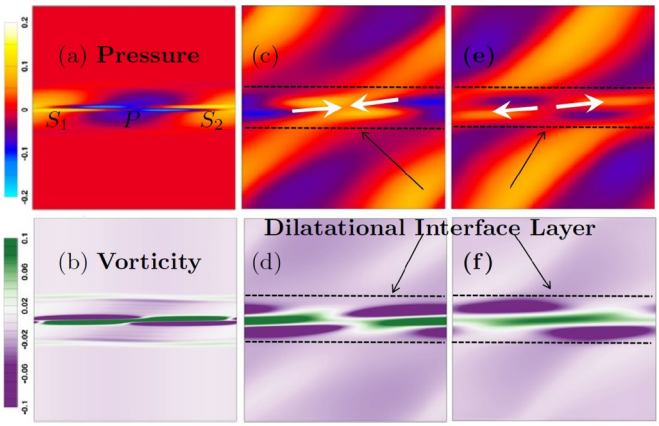

FIG. 5. KHI development in the compressible ($M_c = 1.2$) case: *Stage 1*—initial development [(a), (b)]; *Stage 2*—vortex reversal [(c)–(f)]; dashed lines demarcate the dilatational interface layer.

Stage 2. The second stage behavior is markedly different in the compressible case as p' and u_2' evolve according to wave equations. Around P: (i) the magnitude of u_2' reduces gradually and changes sign leading to the reversal of the vortices in the Q_2 and Q_4 quadrants to counterclockwise; (ii) similar reversal of vortices in Q_1 and Q_3 to clockwise; and (iii) gradual increase in pressure. Thus, *vortex reversal rather than merging dominates* the second stage.

During the reversal process, positive pressure and counterclockwise vortex prevail at P, shown in Figs. 5(c) and 5(d). With the passage of time, the pressure at P returns to negative values accompanied by clockwise vorticity in the Q_2 and Q_4 quadrants and counterclockwise in the Q_1 and Q_3 quadrants as seen in Figs. 5(e) and 5(f). Most importantly, the reversals preclude the central KHI mechanism in compressible flows—steady positive feedback between the clockwise vortex and low pressure at P. The effect of the reversal of the vortex roll-up is shown in Fig. 2(d), where the level of circulation diminishes as the Mach number increases. A similar reversal, but in the opposite direction occurs at S_1 and S_2. Thus, this stage is now identified as the *first vortex reversal stage* with no roll-up.

Stage 3. The *asymptotic* stage is marked by periodic reversals until nonlinear or viscous processes intervene. There is no steady entrainment and thus the circulation remains small.

Outer regions. Although M_g is smaller than unity in the outer regions, the behavior here is not similar to that in the incompressible flow. Pressure waves generated within the DIL propagate through these regions dominating the flow features. At any given point, the velocity is nearly periodic and this leads to very little mixing even in the low M_g regions.

In this work, we uncover the physical mechanism of the KHI suppression in compressible flows through the pressure-velocity interaction dynamics. The contrast between incompressible and compressible cases is exhibited in Fig. 6. The most crucial dynamics occur in the vicinity of P. A low-pressure region forms around P and clockwise and counterclockwise vortices form in diagonally opposite quadrants as seen in Figs. 6(a) and 6(b). The behavior in the *second stage* is determined by the evolution equations and hence markedly

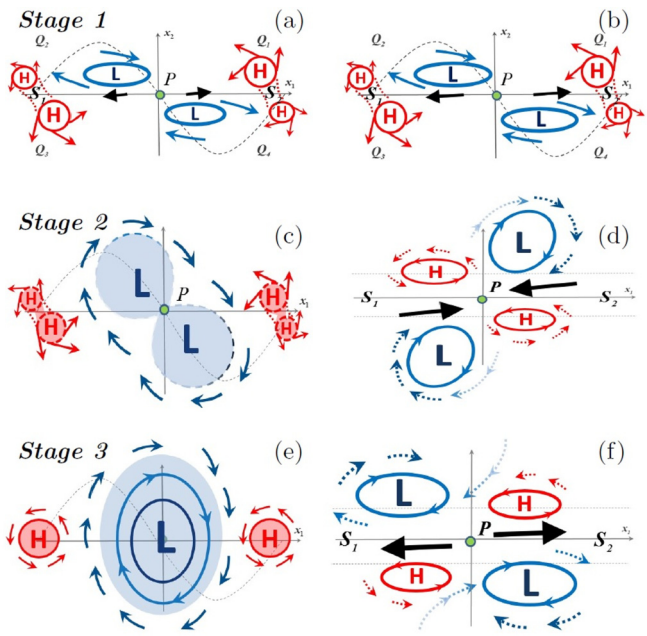

FIG. 6. Schematic representation of contrasting the stages of the KHI development in the incompressible (left) against the compressible (right) flows.

different in the two cases. In the incompressible case, the velocity field mediates a steady positive-feedback interaction between the clockwise vortex and the negative pressure field causing mutual intensification and ultimately triggering the KHI [Fig. 6(c)]. On the other hand, compressibility engenders the formation of a dilatational interface layer which acts as a barrier between two streams. Within this interface, the compressible velocity field is inherently oscillatory, resulting in vorticity and pressure field reversals, precluding positive-feedback growth [Fig. 6(d)]. We find that the influence of compressibility sets in gradually with increasing Mach number rather than a distinct bifurcation. At the *final stage*, the incompressible case features a solid body vortex rotation in the low-pressure region around P [Fig. 6(e)]. In stark contrast, the compressible interface features mostly oscillatory fluid motion that cannot sustain vorticity or mixing between the two streams as illustrated by the dashed vortex lines in Figs. 6(d)–6(f). The gradual change in linear stability behavior with increasing Mach numbers and subsequent nonlinear effects will be addressed in detail in future works.

In summary, the action of pressure leads to shear-driven stirring action between the two streams at low speeds, and a dilatation-driven oscillatory motion of the interface at high speeds. While stirring leads to mixing (instability), oscillations maintain segregation (stabilization) between the two streams. The findings can potentially be generalized to a variety of high-speed shear flows including hypersonic boundary layers and jets. In particular, the present analysis can be extended to examine supersonic plasma jets in astrophysical flows.

Acknowledgments. We thank the anonymous reviewers for their constructive remarks and comments for improving an earlier version of this manuscript.

[1] H. Helmholtz, Uber discontinuierliche flssigkeits-bewegungen (on the discontinuous movements of fluids), Philos. Mag. **36**, 1798 (1868).
[2] W. Thomson (Lord Kelvin), Hydrokinetic solutions and observations, Philos. Mag. **42**, 362 (1871).
[3] L. Rayleigh, On the stability of certain fluid motions, Proc. Math. Soc. London **s1-19**, 67 (1887).
[4] C. P. Caulfield and W. R. Peltier, The anatomy of mixing transition in homogeneous and stratified free shear, J. Fluid Mech. **413**, 1 (2000).
[5] H. Baty and R. Keppens, Interplay between Kelvin-Helmholtz and current-driven instabilities in jets, Astrophys. J. **580**, 800 (2002).
[6] C. L. Gardner and S. J. Dwyer, Numerical simulation of the XZ tauri supersonic astrophysical jet, Acta Math. Sci. **29**, 1677 (2009).
[7] H. Baty and R. Keppens, Kelvin-Helmholtz disruptions in extended magnetized jet flows, Astron. Astrophys. **447**, 9 (2006).
[8] P. Garaud and D. N. C. Lin, On the evolution and stability of a protoplanetary disk dust layer, Astrophys. J. **608**, 1050 (2004).
[9] A. Miura, Self-Organization in the Two-Dimensional Kelvin-Helmholtz Instability, Phys. Rev. Lett. **83**, 1586 (1999).
[10] H. Hasegawa, M. Fujimoto, T. D. Phan, H. Reme, A. Balogh, M. W. Dunlop, C. Hashimoto, and R. TanDokoro, Transport of solar wind into Earth's magnetosphere through rolled-up Kelvin-Helmholtz vortices, Nature (London) **430**, 755 (2004).
[11] C. Foullon, E. Verwichte, V. M. Nakariakov, K. Nykyri, and C. J. Farrugia, Magnetic Kelvin-Helmholtz instability at the sun, Astrophys. J. Lett. **729**, L8 (2011).
[12] H. Nagano, Effect of finite ion Larmor radius on the Kelvin-Helmholtz instability of the magnetopause, Planet. Space Sci. **27**, 881 (1979).
[13] A. Miura, Anomalous transport by magnetohydrodynamic Kelvin-Helmholtz instabilities in the solar wind-magnetosphere interaction, J. Geophys. Res. **89**, 801 (1984).
[14] J. W. Miles, On the generation surface waves by shear flows. 3. Kelvin-Helmholtz instability, J. Fluid Mech. **6**, 583 (1959).
[15] R. Keppens, G. Toth, R. H. J. Westermann, and J. P. Goedblod, Growth and saturation of the KelvinHelmholtz instability with parallel and antiparallel magnetic fields, J. Plasma Phys. **61**, 1 (1999).
[16] L. D. Landau, On the stability of tangential discontinuities in a compressible fluid, Akad. Kauk. L. S. S. S. R. Comptes Rendus (Doklndy) **44**, 139 (1944).
[17] S. Chandrasekhar, *Hydrodynamic and Hydromagnetic Stability* (Oxford Clarendon Press, London, 1961).
[18] P. G. Drazin and N. Howard, Hydrodynamic stability of parallel flow of inviscid fluid, Adv. Appl. Mech. **9**, 1 (1966).
[19] W. Blumen, Shear layer instability of an inviscid compressible fluid, J. Fluid Mech. **40**, 769 (1970).
[20] D. Papamoschou and A. Roshko, The compressible turbulent shear layers: An experimental study, J. Fluid Mech. **197**, 453 (1988).
[21] T. L. Jackson and C. E. Grosch, Absolute/convective instabilities and the convective Mach number in a compressible mixing layer, Phys. Fluids A **2**, 949 (1990).
[22] M. Lessen, J. A. Fox, and H. M. Zien, On the inviscid instability of laminar mixing of two parallel streams of a compressible fluid, J. Fluid Mech. **23**, 355 (1965).
[23] G. Chimonas, The extension of the Miles-Howard theorem to compressible fluids, J. Fluid Mech. **43**, 833 (1970).
[24] W. Blumen, P. G. Drazin, and D. F. Billings, Shear layer instability of an inviscid compressible fluid. Part 2, J. Fluid Mech. **71**, 305 (1975).
[25] P. G. Drazin and A. Davey, Shear layer instability of an inviscid compressible fluid. Part 3, J. Fluid Mech. **82**, 255 (1977).
[26] T. L. Jackson and C. E. Grosch, Inviscid spatial stability of a compressible mixing layer, J. Fluid Mech. **208**, 609 (1989).
[27] P. G. Drazin and W. Reid, *Hydrodynamic Stability* (Cambridge University Press, New York, 1981).
[28] P. J. Schmid and D. S. Henningson, *Stability and Transition in Shear Flows* (Springer-Verlag, Berlin, 2001).
[29] R. Betchov and W. O. Criminale, *Stability of Parallel Flows*, 1st ed. (Academic, New York, 1967).
[30] L. Howarth, Concerning the effect of compressibility on laminar boundary layers and their separation, Proc. R. Soc. London, Ser. A **194**, 16 (1948).
[31] P. J. Schmid, Nonmodal stability theory, Annu. Rev. Fluid Mech. **39**, 129 (2007).
[32] M. Karimi, Compressibility Effects on the Kelvin-Helmholtz Instability and Mixing Layer Flows, PhD. thesis, Texas A&M University, 2015.
[33] S. Sarkar, The stabilizing effect of compressibility in turbulent shear flow, J. Fluid Mech. **282**, 163 (1995).
[34] A. Lifschitz and E. Hameiri, Local stability conditions in fluid dynamics, Phys. Fluids A **3**, 2644 (1991).
[35] D. Livescu and C. K. Madnia, Small scale structure of homogeneous turbulent shear flow, Phys. Fluids **16**, 2864 (2004).
[36] G. Kumar, R. L. Bertsch, and S. S. Girimaji, Stabilizing action of pressure in homogeneous compressible shear flows: Effect of Mach number and perturbation obliqueness, J. Fluid Mech. **760**, 540 (2014).
[37] G. Kumar, S. S. Girimaji, and J. Kerimo, Weno-enhanced gas-kinetic scheme for direct simulations of compressible transition and turbulence, J. Comput. Phys. **234**, 499 (2012).
[38] Z. Xie and S. S. Girimaji, Instability of Poiseuille flow at extreme Mach numbers: Linear analysis and simulations, Phys. Rev. E **89**, 043001 (2014).
[39] S. A. Ragab and J. L. Wu, Linear instabilities in two-dimensional compressible mixing layers, Phys. Fluids A **1**, 957 (1989).
[40] M. Samimy and G. S. Elliot, Effects of compressibility on the characteristics of free shear layers, AIAA J. **28**, 439 (1990).
[41] N. D. Sandham and W. C. Reynolds, Three-dimensional simulations of large eddies in the compressible mixing layer, J. Fluid Mech. **224**, 133 (1991).
[42] T. Rossmann, M. G. Mungal, and R. K. Hanson, Evolution and growth of large-scale structures in high compressibility mixing layers, J. Turb. **3**, N9 (2002).
[43] C. Pantano and S. Sarkar, A study of compressibility effects in the high-speed turbulent shear layer using dircet simulation, J. Fluid Mech. **451**, 329 (2002).
[44] A. J. Smits and J.-P. Dussauge, *Turbulent Shear Layers in Supersonic Flows*, 2nd ed. (Springer, New York, 2006).
[45] R. D. Moser and M. M. Rogers, The three-dimensional evolution of a plane mixing layer: Pairing and transition to turbulence, J. Fluid Mech. **247**, 275 (1993).
[46] W. R. Peltier and C. P. Caulfield, Mixing efficiency in stratified shear flows, Annu. Rev. Fluid Mech. **35**, 135 (2003).